Radiative corrections to the hyperfine-structure splitting of hydrogenlike systems

P. Sunnergren,[1] H. Persson,[1] S. Salomonson,[1] S. M. Schneider,[2] I. Lindgren,[1] and G. Soff [3]
[1]*Department of Physics, Chalmers University of Technology and the Göteborg University, SE-412 96 Göteborg, Sweden*
[2]*Institut für Theoretische Physik, Johann Wolfgang Goethe Universität, Postfach 111 932, D-60054 Frankfurt am Main, Germany*
[3]*Institut für Theoretische Physik, Technische Universität Dresden, Mommsenstraße 13, D-01062 Dresden, Germany*
(Received 20 February 1998)

We present a complete calculation of the leading nonrecoil radiative corrections to the $1s$ hyperfine-structure splitting of highly charged hydrogenlike ions. In particular, we have investigated how the radiative corrections for ions with a high nuclear charge number Z are affected by using an extended nuclear magnetization. We also present the first complete evaluation of the Wichmann-Kroll part of the vacuum polarization correction to all orders in $(Z\alpha)$. To unambiguously incorporate this effect we have also calculated the vacuum polarization correction to the measured nuclear magnetic moment. Total theoretical results are collected for the experimentally interesting ions $^{209}Bi^{82+}$, $^{207}Pb^{81+}$, $^{185}Re^{74+}$, and $^{165}Ho^{66+}$. Also the low-Z region is considered in order to compare with the known part of the $(Z\alpha)$ expansion. [S1050-2947(98)02608-0]

PACS number(s): 31.30.Gs, 31.30.Jv, 31.15.Ar

I. INTRODUCTION

The so-called satellite structure of atomic spectral lines was an experimentally long known fact when Pauli first assigned it to the different orientations of the valence-electron in the magnetic field of a nucleus [1]. Because of its relative smallness when compared to other structures in atomic spectra, this splitting became known as the hyperfine structure.

As a consequence of recent modern experimental developments, ways are opened to study atoms in quite unnatural states, e.g., highly charged heavy ions, in the hope to uncover new effects or to verify accepted theories in very extreme situations. Investigations of the atomic structure of very highly charged heavy ions are now feasible, for example, at GSI (Germany), LLNL (USA), and RIKEN (Japan).

The first measurement of the ground-state hyperfine-structure splitting of a one-electron ion with high nuclear charge number Z was performed in 1993 at GSI. The wavelength of the hyperfine-structure splitting in $^{209}Bi^{82+}$ was found to be $\lambda_{\text{expt.}}=243.87(4)$ nm [2], where the error is mainly due to the uncertainty in the ion velocity. This corresponds to a splitting energy of $\Delta E_{\text{expt.}}=5.0840(8)$ eV.

The high relative accuracy of the measurement in Bi implied a first testing scenario of QED corrections in the combined presence of a strong magnetic field and a strong Coulomb field of a heavy nucleus. This pioneering measurement has been followed by similar experiments on other ions [3–5] and several theoretical investigations on this subject [6–10].

In contrast to hydrogen, the nuclear structure plays a much more vital role for heavy ions. Compared to a proton, the size of a heavy nucleus with $Z\simeq 80$ is about five times larger and in addition the Bohr radius of the $1s$ electron is reduced by a factor of $1/Z$. To theoretically obtain the correct splitting between two hyperfine levels in H-like systems, the first step is to calculate the dominating first-order hyperfine interaction. The major nuclear size effect on this first-order calculation is the extended nuclear charge, which can be handled using realistic charge distributions (e.g., Fermi distributions) [11]. A more limiting uncertainty comes from the extended nuclear magnetization distribution, the Bohr-Weisskopf effect [12], which has received considerable interest lately [9,13–16]. For hydrogenlike Bi this effect is $-0.107(7)$eV [15], which can be compared to the extended nuclear charge effect of $-0.6482(7)$eV.

Beyond these effects also the one-photon self-energy (SE) and vacuum-polarization (VP) corrections have to be added. For low nuclear charge numbers Z it is appropriate to make a series expansion in $(Z\alpha)$ to obtain the leading radiative corrections. The known part of the $(Z\alpha)$ expansion for the one-photon QED effects [17–26] can be summarized as

$$\Delta E^{(2)}_{\text{QED}}=\Delta E_F\frac{\alpha}{\pi}(F^{(2)}_{\text{SE}}+F^{(2)}_{\text{VP}}), \tag{1}$$

where ΔE_F is the nonrelativistic (point-nucleus) Fermi splitting energy [27] and where

$$F^{(2)}_{\text{SE}}=\frac{1}{2}+\left(\ln 2-\frac{13}{4}\right)\pi(Z\alpha)+\left[-\frac{8}{3}\ln^2(Z\alpha)+\left(-\frac{37}{36}+\frac{16}{3}\ln 2\right)\ln(Z\alpha)+H^{(2)}_{\text{SE}}\right](Z\alpha)^2 \tag{2}$$

and

$$F^{(2)}_{\text{VP}}=\frac{3}{4}\pi(Z\alpha)+\left[-\frac{8}{15}\ln(Z\alpha)+H^{(2)}_{\text{VP}}\right](Z\alpha)^2. \tag{3}$$

The terms $H^{(2)}_{\text{SE}}$ and $H^{(2)}_{\text{VP}}$ have recently been evaluated to leading orders [23–26] and can be expressed as

$$H^{(2)}_{\text{SE}}=17.122+\left[\left(-5\ln 2+\frac{191}{16}\right)\pi\ln(Z\alpha)\right](Z\alpha)+\cdots \tag{4}$$

and

$$H^{(2)}_{\text{VP}}=-\frac{8}{15}\ln 2+\frac{34}{225}-\frac{13}{24}\pi\ln(Z\alpha)(Z\alpha)+\cdots. \tag{5}$$

From Lamb-shift calculations it is known that the $(Z\alpha)$ expansion of the SE correction has increasingly worse convergence properties for increasing Z. For the interesting region of $Z\simeq 80$ the effective coupling constant to the Coulomb field is $(Z\alpha)\simeq 0.6$ and no reasonable result can be obtained from the badly alternating series expansion. A similar behavior shows up for the hyperfine structure.

In this paper we present a calculation of the leading nonrecoil QED corrections (of order α), to all orders in $(Z\alpha)$, for the $1s$ state in hydrogenlike ions. The paper includes a detailed description of how we calculate the self-energy and the vacuum-polarization effects. To unambiguously incorporate the latter effect we have also included the VP correction to the measured nuclear magnetic moment. Furthermore, we have investigated the effect of having an extended nuclear magnetization (as well as an extended nuclear charge distribution) when calculating the radiative corrections. In Sec. II we discuss the first-order hyperfine interaction and in Secs. III and IV the SE and the VP corrections are considered. In the final section we present numerical results for some experimentally interesting highly charged ions as well as results for low Z where a comparison with the $(Z\alpha)$ expansion is meaningful.

II. FIRST-ORDER HYPERFINE INTERACTION

The first step in calculating the hyperfine-structure splitting of a given system is to evaluate the first-order perturbation theory result. The relativistic interaction Hamiltonian is given by (units where $\hbar=\epsilon_0=c=1$ will be used throughout the paper)

$$\hat{H}_{\rm int}=e\,\boldsymbol{\alpha}\cdot\mathbf{A}(\mathbf{r}), \tag{6}$$

where $\mathbf{A}(\mathbf{r})$ denotes the nuclear magnetic vector potential. Considering only linear terms in the hyperfine interaction, an s electron is not affected by the angular variation (deformation) of the nuclear charge distribution. One can therefore assume a spherically symmetric nuclear Coulomb potential in the Dirac equation. The electron spinor can then be separated into an angular and a radial part as

$$\psi(\mathbf{r})=\begin{pmatrix} f(r)\chi_\kappa^m(\hat{r}) \\ ig(r)\chi_{-\kappa}^m(\hat{r})\end{pmatrix}=\frac{1}{r}\begin{pmatrix} F(r)\chi_\kappa^m(\hat{r}) \\ iG(r)\chi_{-\kappa}^m(\hat{r})\end{pmatrix}, \tag{7}$$

where $f(r)$ and $g(r)$ are the large and small radial components of the wave function, respectively, and $\chi_\kappa^m(\hat{r})$ is the ls-coupled spin-angular function. The Dirac equation then leads to the coupled radial equations

$$\frac{d}{dr}G(r)=\frac{\kappa}{r}G(r)-[E-m-V(r)]F(r), \tag{8}$$

$$\frac{d}{dr}F(r)=-\frac{\kappa}{r}F(r)+[E+m-V(r)]G(r). \tag{9}$$

For a point nucleus these equations can be solved analytically, but for a parametrized nuclear charge distribution, e.g., a Fermi-like distribution or a model-independent Fourier-Bessel expansion of the charge distribution, they have to be solved numerically.

Since the interaction Hamiltonian acts on the nuclear wave function as well as on the electron wave function, one has to consider the wave function of the coupled system. In zeroth order this wave function is given by

$$\Psi_{Fm_F}^{(0)}(\mathbf{r},\mathbf{R})=\sum_{m_I,m_j}\left(\begin{array}{cc|c} I & j & F \\ m_I & m_j & m_F\end{array}\right)\psi_{jm_j}^{(0)}(\mathbf{r})\,\phi_{Im_I}^{(0)}(\mathbf{R}), \tag{10}$$

where $\mathbf{R}$ denotes the nuclear coordinates and I, j, and F denote the angular momentum quantum numbers of the nucleus, the electron, and the coupled system. The m_i are the magnetic projection quantum numbers. In the magnetic point-dipole approximation, the vector potential is given by (the nuclear magnetic moment is denoted by $\boldsymbol{\mu}$)

$$\mathbf{A}(\mathbf{r})=\frac{\boldsymbol{\mu}\times\mathbf{r}}{4\pi r^3}=g_I\mu_N\frac{\mathbf{I}\times\mathbf{r}}{4\pi r^3}, \tag{11}$$

where g_I is the nuclear g factor, μ_N denotes the nuclear magneton, and $\mathbf{I}$ is the nuclear spin operator. The first-order energy splitting between the ground-state hyperfine-structure levels can, after angular integrations, be expressed as

$$\Delta E^1=-\frac{eg_I\mu_N}{4\pi}\frac{2}{3}[F_2(F_2+1)-F_1(F_1+1)]2 \times\int r^2dr\frac{f(r)g(r)}{r^2}. \tag{12}$$

Here, $F_1=I-1/2$ and $F_2=I+1/2$ are the total angular quantum numbers of the lower and upper hyperfine level, respectively. It should be noted that the effect of an extended spherical nuclear charge distribution can be included in the Dirac equation above and thus enters in the radial functions $f(r)$ and $g(r)$.

For later convenience we also transform the relevant first-order corrections into momentum space. In momentum space the electron wave function is given by

$$\psi_a(\mathbf{p})=\frac{1}{(2\pi)^{3/2}}\int d^3\mathbf{r}e^{-i\mathbf{p}\cdot\mathbf{r}}\psi_a(\mathbf{r})=\begin{pmatrix} P(p)\chi_\kappa^m(\hat{p}) \\ Q(p)\chi_{-\kappa}^m(\hat{p})\end{pmatrix}. \tag{13}$$

The interaction potential in momentum space depends on the difference $\mathbf{q}=\mathbf{p}-\mathbf{p}'$, where $\mathbf{p}$ and $\mathbf{p}'$ are the outgoing and incoming momenta, respectively. It has the form

$$\mathbf{A}(\mathbf{q})=\frac{1}{(2\pi)^3}\int d^3\mathbf{r}e^{-i\mathbf{q}\cdot\mathbf{r}}\mathbf{A}(\mathbf{r})=-\frac{i}{(2\pi)^3}\frac{\boldsymbol{\mu}\times\mathbf{q}}{\mathbf{q}^2}. \tag{14}$$

The first-order hyperfine energy in momentum space is given by the integral

$$E^1_{F,m_F}=\frac{-ie}{(2\pi)^3}\times\int d^3\mathbf{p}d^3\mathbf{p}'\Psi^\dagger_{Fm_F}(\mathbf{p})\frac{\boldsymbol{\alpha}\cdot[\boldsymbol{\mu}\times(\mathbf{p}-\mathbf{p}')]}{(\mathbf{p}-\mathbf{p}')^2}\Psi_{Fm_F}(\mathbf{p}'), \tag{15}$$

where we implicitly also assume an integration over nuclear coordinates, which in practice only leads to an angular factor. Also in the rest of the paper, when we have equations involving both electron and nuclear quantities, the integrations over the nuclear coordinates will be implicitly assumed. To separate out the angular dependencies of the denominator in the Fourier transform of the vector potential, we use the general expansion of a function of $\cos\vartheta$, where ϑ is the angle between $\mathbf{p}$ and $\mathbf{p}'$,

$$V(p,p',\cos\vartheta)=\sum_{l=0}^{\infty}(2l+1)V_l(p,p')\mathbf{C}^l(\hat{p})\cdot\mathbf{C}^l(\hat{p}'). \tag{16}$$

Here the $\mathbf{C}^l$ tensor is related to the spherical harmonics Y^l_m as $C^l_m=\sqrt{4\pi/(2l+1)}Y^l_m$. The expansion coefficients $V_l(p,p')$ are given by

$$V_l(p,p')=\frac{1}{2}\int_{-1}^{1}d(\cos\vartheta)V(p,p',\cos\vartheta)P_l(\cos\vartheta), \tag{17}$$

where $P_l(\cos\vartheta)$ is the Legendre polynomial of order l. For the ground state we get contributions from the $l=0$ and the $l=1$ terms only, and the hyperfine splitting can be written as

$$\Delta E^1=-\frac{eg_I\mu_N}{4\pi}\frac{2}{3}[F_2(F_2+1)-F_1(F_1+1)]\times 2\frac{2}{\pi}\int dpp^2\int dp'p'^2[p'V_0(p,p')-pV_1(p,p')]P(p)Q(p'), \tag{18}$$

where

$$V_0(p,p')=\frac{1}{2}\left[\frac{1}{2pp'}\ln\left(\frac{(p+p')^2}{(p-p')^2}\right)\right], \tag{19}$$

$$V_1(p,p')=\frac{1}{2}\left[-\frac{1}{pp'}+\frac{p^2+p'^2}{4p^2p'^2}\ln\left(\frac{(p+p')^2}{(p-p')^2}\right)\right], \tag{20}$$

are the expansion coefficients. Note that we have here considered the point-dipole case, but when treating a more general operator the integration in Eq. (17) is performed numerically.

One of the principal aims of this paper is to investigate how the radiative corrections are affected by using an extended nuclear magnetization. To achieve this in a straightforward manner we have adopted a model for the magnetic moment distribution suggested by Finkbeiner *et al.* [13]. In this model a spherically symmetric distribution is assumed for the nuclear magnetic moment $\mathbf{M}(R)=\boldsymbol{\mu}w(R)$. The density function is given by $w(R)=k_nR^n$ for the interior of the nucleus and $w(R)=0$ for the outside of the nucleus, n is the model parameter, and k_n normalizes the distribution to the experimental magnetic moment. The effective radial dependence, which replaces a factor $1/r^2$ in Eq. (11), is then given by

$$V_{\rm eff}(r)=\frac{1}{r^2}\left(\frac{r}{R_0}\right)^{n+3},\quad r\leqslant R_0,$$

$$V_{\rm eff}(r)=\frac{1}{r^2},\quad r>R_0, \tag{21}$$

where R_0 is the nuclear radius. With this parametrization we can consider different magnetic moment distributions, ranging from a homogeneous distribution ($n=0$) up to the shell model ($n=\infty$) where the magnetic moment is located at the nuclear surface.

For bismuth we have further employed the dynamical proton model (DPM) of Labzowsky *et al.* [16]. In the DPM the valence proton of the bismuth nucleus is treated as a Dirac particle bound in the Woods-Saxon potential of the lead core. The first-order hyperfine splitting is then given as a vector-photon exchange between the electron and the proton,

$$\Delta E^1_{\rm DPM}=\alpha[F_2(F_2+1)-F_1(F_1+1)]\frac{(2\kappa)(2K)}{(4\kappa^2-1)(4K^2-1)}\times\int r^2dr\int R^2dR\frac{x_<}{x_>^2}[2f_\kappa(r)g_\kappa(r)]\times[2f_K(R)g_K(R)], \tag{22}$$

where $x_<$ ($x_>$) is the smallest (largest) of r and R. The kappa values for the electron and proton are denoted by κ and K, respectively. The calculations become identical with the corresponding ones for the two-electron Lamb shift [28] with one of the electron wave functions replaced by the proton wave function.

In the rest of this paper, we will state all formulas and equations assuming the point-dipole model. Introducing the extended nuclear magnetization only leads to minor modifications of the expressions.

III. THE SELF-ENERGY CORRECTIONS

The Feynman diagrams for the one-photon radiative corrections can be divided into vacuum polarization [Figs. 1(b) and 1(c)] and self-energy [Fig. 1(d) and 1(e)] parts. The expressions for the one-photon effects can be derived in a formal way, using the S-matrix formalism and the Gell-Mann-Low-Sucher formula [29,30],

$$\Delta E=\lim_{\eta\to 0}\frac{1}{2}i\eta[3\langle a|S^{(3)}_\eta|a\rangle-3\langle a|S^{(2)}_\eta|a\rangle\langle a|S^{(1)}_\eta|a\rangle], \tag{23}$$

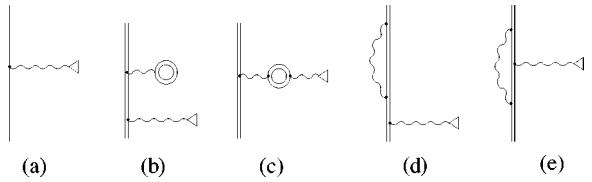

FIG. 1. Feynman diagrams representing the first-order interaction (a) and the one-photon radiative corrections (b)–(e) to the hyperfine splitting. The triangle represents the magnetic interaction with the nucleus.

where η is the adiabatic switching parameter. Here, the second term represents products of disconnected lower-order diagrams.

An alternative way of deriving the QED corrections in the presence of an external vector potential, which gives expressions identical to those derived from Eq. (23), is to perturb the first-order Coulomb self-energy with the magnetic potential, as summarized in [31]. In first-order in the magnetic potential $\mathbf{A}(\mathbf{r})$, the binding energy of the electron E_a, the reference wave function $|a\rangle$, and the propagator for the bound electron S_F are modified as follows:

$$E_a \to E_a + \langle a|e\boldsymbol{\alpha}\cdot\mathbf{A}(\mathbf{r})|a\rangle + \cdots, \tag{24}$$

$$|a\rangle \to |a\rangle + \sum_{E_m \neq E_a} \frac{|m\rangle\langle m|e\boldsymbol{\alpha}\cdot\mathbf{A}(\mathbf{r})|a\rangle}{E_a - E_m} + \cdots = |a\rangle + |\delta a\rangle + \cdots, \tag{25}$$

$$S_F(\boldsymbol{x}_2,\boldsymbol{x}_1;z) \to S_F(\boldsymbol{x}_2,\boldsymbol{x}_1;z) + \int d^3\boldsymbol{x}_3 S_F(\boldsymbol{x}_2,\boldsymbol{x}_3;z) e\boldsymbol{\alpha}\cdot\mathbf{A}(\boldsymbol{x}_3) S_F(\boldsymbol{x}_3,\boldsymbol{x}_1;z) + \cdots. \tag{26}$$

The wave-function modification term, originating from the replacement Eq. (25), takes the form

$$\Delta E_{\mathrm{SE}}^{\mathrm{WF}} = \sum_t \frac{\langle a|(\Sigma_{\mathrm{bou}} - \delta m)|t\rangle\langle t|e\boldsymbol{\alpha}\cdot\mathbf{A}|a\rangle}{E_a - E_t}, \tag{27}$$

with $E_t \neq E_a$. Here Σ_{bou} denotes the unrenormalized bound self-energy operator and δm the mass counter term.

The vertex correction, replacement Eq. (26), leads to the following expression:

$$\Delta E_{\mathrm{SE}}^{\mathrm{VE}} = \langle a|e\boldsymbol{\Lambda}\cdot\mathbf{A}|a\rangle, \tag{28}$$

where $\boldsymbol{\Lambda}$ is the bound vector vertex function. For the binding energy term, replacement Eq. (24), the formula reads as follows:

$$\Delta E_{\mathrm{SE}}^{\mathrm{BE}} = \langle a|e\boldsymbol{\alpha}\cdot\mathbf{A}|a\rangle \times \langle a|\left(\frac{\partial}{\partial E}\Sigma(E)\right)_{E=E_a}|a\rangle. \tag{29}$$

To handle the divergences present in these three terms, we expand the self-energy and the vertex operator in the nuclear Coulomb potential. The mass and charge divergences will then be isolated in the lowest-order terms and can be canceled analytically between different diagrams. This procedure is done working in momentum space and using dimensional regularization for the divergent integrals. The finite higher-order terms are then calculated in coordinate space by taking the difference between the full unrenormalized expression and the divergent parts in the expansion.

We start here by considering the self-energy and the vertex operator using dimensional regularization. The expressions derived will be used later when discussing the calculation of the three different contributions. Note that in the expressions for $\Sigma(p)$ and $\Lambda_\mu(p,p')$, the notation p (k) denotes the four-momentum whereas it indicates the absolute values $p=|\mathbf{p}|$ $(k=|\mathbf{k}|)$ elsewhere in the paper.

The free self-energy operator reads in Feynman gauge

$$\Sigma(p) = -i4\pi\alpha \int \frac{d^4k}{(2\pi)^4}\gamma^\mu \frac{\not{p}-\not{k}+m}{(p-k)^2-m^2}\gamma_\mu \frac{1}{k^2}, \tag{30}$$

which after mass renormalization can be written as [32]

$$\Sigma_{\mathrm{ren}}^{\mathrm{mass}}(p) = \Sigma(p) - \delta m = -\frac{\alpha}{4\pi}\left\{(\not{p}-m)\left[\Delta + 2 + \frac{\rho}{1-\rho}\left(1 + \frac{2-\rho}{1-\rho}\ln\rho\right)\right] + \frac{m\rho}{1-\rho}\left(1 - \frac{2-3\rho}{1-\rho}\ln\rho\right)\right\}. \tag{31}$$

Here $\Delta = 2/\varepsilon - \gamma_E + \ln 4\pi$ is the ultraviolet part of the charge renormalization constant after dimensional regularization, ε is the dimensional regularization parameter, and γ_E is Euler's constant. We have further introduced the dimensionless variable

$$\rho = \frac{m^2 - E^2 + \mathbf{p}^2}{m^2} = -\frac{(\not{p}-m)(\not{p}+m)}{m^2}, \tag{32}$$

which is positive definite for a bound electron. The mass-renormalized self-energy Eq. (31) is finite in the infrared limit since we only extract the ultraviolet part of the charge renormalization constant. Only when extracting the full charge renormalization constant will there appear an explicit infrared divergence [32]. This is also the case for the vertex operator and it is therefore sufficient to cancel the ultraviolet divergency, which vanishes due to the Ward identity, between these two operators to obtain finite expressions.

Taking into account the energy dependence of ρ, the derivative of the free self-energy operator with respect to the energy is given by

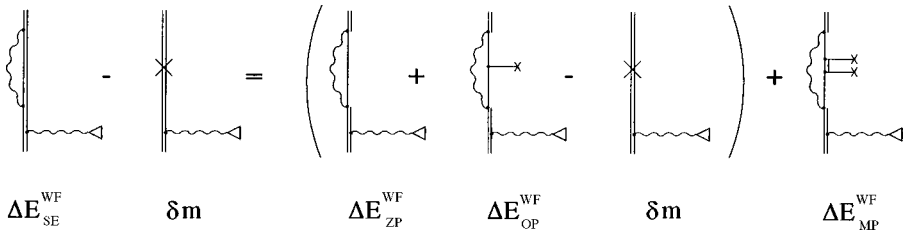

FIG. 2. Feynman graphs representing the wave-function correction. In order to isolate divergences, the internal self-energy electron propagator is expanded in the nuclear Coulomb potential, which is denoted by a horizontal line with a cross. The divergent zero-potential, one-potential, and the mass-counter term are grouped together. The remaining many-potential term is finite.

$$\frac{\partial\Sigma(p)}{\partial E}=-\frac{\alpha}{4\pi}\left\{\gamma_0\left[\Delta+2+\frac{\rho}{1-\rho}\left(1+\frac{2-\rho}{1-\rho}\ln\rho\right)\right]+\frac{\not p}{m^2}\left[-\frac{2E}{(1-\rho)^2}\left(3-\rho+\frac{2}{1-\rho}\ln\rho\right)\right]+\frac{8E}{m(1-\rho)}\left[1+\frac{1}{1-\rho}\ln\rho\right]\right\}. \tag{33}$$

This expression is needed for the computation of the free-electron part of the binding-energy correction.

Finally, the vertex-correction operator for a free electron is given by

$$\Lambda_\mu(p,p')=-i4\pi\alpha\int\frac{d^4k}{(2\pi)^4}\gamma_\nu\frac{\not p-\not k+m}{(p-k)^2-m^2}\times\gamma_\mu\frac{\not p'-\not k+m}{(p'-k)^2-m^2}\gamma^\nu\frac{1}{k^2}. \tag{34}$$

By using the coefficient functions C_{ij}, which are functions of p, p' and given by Feynman parameter integrals, as defined in Ref. [32], one finds the complete covariant vertex operator

$$\Lambda_\mu(p,p')=\frac{\alpha}{4\pi}\{\gamma_\mu[4C_{24}-2+2m^2C_0-4pp'(C_0+C_{11}+C_{12}+C_{23})-2p^2(C_{11}+C_{21})-2p'^2(C_{12}+C_{22})]+\not p p_\mu[4(C_{11}+C_{21})]+\not p p'_\mu[4(C_0+C_{11}+C_{12}+C_{23})]+\not p' p_\mu[4(C_0+C_{11}+C_{12}+C_{23})]+\not p' p'_\mu[4(C_{12}+C_{22})]-\not p\gamma_\mu\not p'[2(C_0+C_{11}+C_{12})]-p_\mu[4m(C_0+2C_{11})]-p'_\mu[4m(C_0+2C_{12})]\}. \tag{35}$$

Here, the ultraviolet divergency Δ is contained in the coefficient function C_{24}. The zeroth component of $\Lambda_\mu(p,p')$ enters the wave-function correction term and the vector part is needed for the calculation of the vertex correction part.

To cancel the infrared and ultraviolet divergences, it is appropriate to organize the different terms into two different subgroups, wave-function corrections and vertex plus binding energy corrections, depending on the structure of the divergences in the diagrams.

A. Wave-function corrections

The structure of divergences in the wave-function correction is the same as for the first-order self-energy. We can therefore isolate and subtract the divergences by means of a potential expansion of the self-energy operator into a free self-energy operator (ZP), a one-potential term (OP), and a finite many-potential part (MP); see Fig. 2. The many-potential part is treated in coordinate space in a similar way as in previous works [6,28,33,34]. The divergent zero- and one-potential terms are grouped together with the mass counter term, and by the use of dimensional regularization the finite parts can be extracted and calculated in momentum space [32]. The wave-function correction is thus calculated as two separate parts,

$$\Delta E_{\rm SE}^{\rm WF}=\Delta E_{\rm ZP}^{{\rm WF},p}+\Delta E_{\rm OP}^{{\rm WF},p}+\Delta E_{\rm MP}^{{\rm WF},x}=\Delta E^{{\rm WF},p}+\Delta E_{\rm MP}^{{\rm WF},x}, \tag{36}$$

where p and x indicate that the calculations are performed in momentum and coordinate space, respectively. In the following we will consider the ket-state as the perturbed wave function, but there is of course also a symmetrical diagram where instead the bra-state is perturbed by the hyperfine interaction.

1. The zero- and one-potential parts

In terms of the perturbed wave function,

$$|\delta a\rangle=\sum_{E_m\neq E_a}\frac{|m\rangle\langle m|e\boldsymbol{\alpha}\cdot\mathbf{A}(\mathbf{r})|a\rangle}{E_a-E_m}, \tag{37}$$

the zero- and one-potential terms are given by

$$\Delta E^{\mathrm{WF},p} = \langle a|\Sigma_{\mathrm{zero}}(p) + \Sigma_{\mathrm{one}}(p) - \delta m|\,\delta a\rangle$$
$$= \langle a|\Sigma^{\mathrm{mass}}_{\mathrm{ren}}(p) + \Lambda_0(p,p')V_c(\mathbf{p},\mathbf{p}')|\,\delta a\rangle. \quad (38)$$

Here, $V_c(\mathbf{p},\mathbf{p}')$ is the nuclear Coulomb potential, $\Sigma^{\mathrm{mass}}_{\mathrm{ren}}(p)$ is given by Eq. (31), and $\Lambda_0(p,p')$ is the zeroth component of the vertex function Eq. (35). The ultraviolet divergent parts are cancelled by omitting the term proportional to Δ in these expressions and the remainder of the charge renormalization constant vanishes when adding the zero- and one-potential terms.

To discuss the calculation of the zero-potential part we first separate the tensor structure by writing $\Sigma^{\mathrm{mass}}_{\mathrm{ren}}(p) = a(\rho) + \not{p}b(\rho)$. For the a part, which is diagonal, the angular integrations can be done straightforwardly, which yields

$$C(p) = \int d\Omega\, \psi^\dagger_a(\mathbf{p})\gamma_0\psi_{\delta a}(\mathbf{p}) = P_a P_{\delta a} - Q_a Q_{\delta a}. \quad (39)$$

For the $\not{p}$ term we use the explicit form

$$\not{p} = \begin{pmatrix} E & -\boldsymbol{\sigma}\cdot\mathbf{p} \\ \boldsymbol{\sigma}\cdot\mathbf{p} & -E \end{pmatrix}, \quad (40)$$

together with the identity $\boldsymbol{\sigma}\cdot\mathbf{p}\chi^m_\kappa(\hat{p}) = -p\chi^m_{-\kappa}(\hat{p})$, to obtain

$$D(p) = \int d\Omega\, \psi^\dagger_a(\mathbf{p})\gamma_0\not{p}\psi_{\delta a}(\mathbf{p})$$
$$= E(P_a P_{\delta a} + Q_a Q_{\delta a}) + p(P_a Q_{\delta a} + P_{\delta a} Q_a). \quad (41)$$

The remaining radial integral

$$\int dp p^2 [C(p)a(\rho) + D(p)b(\rho)] \quad (42)$$

is performed numerically using Gauss-Legendre quadrature.

The one-potential part is given by the integral

$$\Delta E^{\mathrm{WF},p}_{\mathrm{OP}} = e\int d^3\mathbf{p}d^3\mathbf{p}'\,\psi^\dagger_a(\mathbf{p})\gamma_0[\,\gamma_0 f_1(p,p',\cos\vartheta) + \not{p} f_2(p,p',\cos\vartheta) + \not{p}' f_3(p,p',\cos\vartheta) + \not{p}\gamma_0\not{p}' f_4(p,p',\cos\vartheta)$$
$$+ f_5(p,p',\cos\vartheta)]V_c(\mathbf{p},\mathbf{p}')\psi_{\delta a}(\mathbf{p}'), \quad (43)$$

where the f_i functions are abbreviations for the coefficient functions in Eq. (35). The angular dependence of the wave functions can be reduced to a dependence on the intermediate angle by utilizing the identity

$$\frac{1}{2j+1}\sum_{m=-j}^{j}\chi^{m\dagger}_\kappa(\hat{p})\chi^m_\kappa(\hat{p}') = \frac{1}{4\pi}P_{|\kappa+1/2|-1/2}(\cos\vartheta), \quad (44)$$

where $P_{|\kappa+1/2|-1/2}(\cos\vartheta)$ is a Legendre polynomial. Performing the matrix multiplication and using this identity we obtain for the $1s$ state

$$4\pi\psi^\dagger_a(\mathbf{p})\gamma_0\Lambda_0(p,p')\psi_{\delta a}(\mathbf{p}') = f_1[PP' + QQ'\cos\vartheta] + f_2[EPP' + pQP' + (pPQ' + EQQ')\cos\vartheta]$$
$$+ f_3[EPP' + p'PQ' + (p'QP' + EQQ')\cos\vartheta] + f_4[E^2PP' + pEQP' + p'EPQ' + pp'QQ'$$
$$+ (pp'PP' + pEPQ' + p'EQP' + E^2QQ')\cos\vartheta] + f_5[PP' - QQ'\cos\vartheta], \quad (45)$$

where $P = P_a(p)$ and $P' = P_{\delta a}(p')$ and similarly for Q. The expression for the one-potential part is thus reduced to a three-dimensional integral over p, p' and $\cos\vartheta$, which is evaluated numerically.

2. The many-potential parts

The many-potential part is convergent and can be calculated straightforwardly in coordinate space from the following expression:

$$\Delta E^{\mathrm{WF},x}_{\mathrm{MP}} = -\frac{\alpha}{\pi}\sum_{l=0}^{\infty}(2l+1)\int kdk\Bigg\{\sum_n \frac{\langle a|\alpha_\mu j_l(kr_3)\mathbf{C}^l|n\rangle\langle n|j_l(kr_2)\mathbf{C}^l\alpha^\mu|\,\delta a\rangle}{E_a - E_n - \mathrm{sgn}(E_n)k} - \sum_q \frac{\langle a|\alpha_\mu j_l(kr_3)\mathbf{C}^l|q\rangle\langle q|j_l(kr_2)\mathbf{C}^l\alpha^\mu|\,\delta a\rangle}{E_a - E_q - \mathrm{sgn}(E_q)k}$$
$$- \sum_{p,q}\frac{\langle a|\alpha_\mu j_l(kr_3)\mathbf{C}^l|p\rangle\langle p|V_c(r_2)|q\rangle\langle q|j_l(kr_1)\mathbf{C}^l\alpha^\mu|\,\delta a\rangle}{[E_a - E_p - \mathrm{sgn}(E_p)k][E_a - E_q - \mathrm{sgn}(E_q)k]}\times F\Bigg\}, \quad (46)$$

where $|n\rangle$ denotes bound electron states and $|p\rangle, |q\rangle$ denote free electron states, and where we have introduced the function F defined by

$$F = 1 + [\mathrm{sgn}(E_p) - \mathrm{sgn}(E_q)]\frac{k}{E_p - E_q}. \quad (47)$$

To compute this contribution, as well as the many-potential parts of the vertex and binding energy corrections, we proceed as follows. The radial and the angular integrations are separated and the angular parts are treated analytically by using the graphical angular momentum coupling scheme as discussed in [35–37]. To generate a complete set of interme-

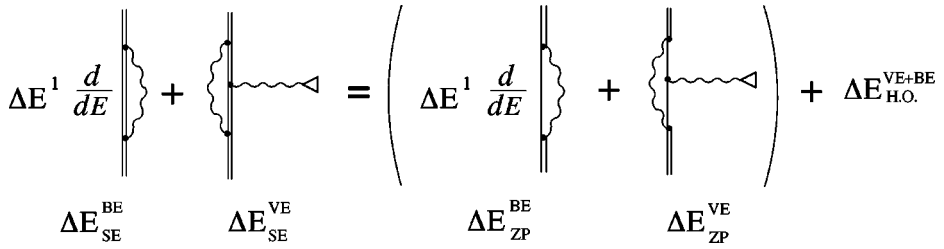

FIG. 3. Feynman graphs representing the binding energy and vertex correction. In this part the divergences occur only in the zero-potential terms, which are grouped together. ΔE^1 denotes the first-order hyperfine splitting.

diate bound- and free-electron states we use the space-discretization method developed by Salomonson and Öster [38]. The resulting wave functions are then numerical discrete valued functions in the chosen r grid. To integrate the overlap with the spherical Bessel functions, which oscillates strongly for high photon momentum, we interpolate the numerical states to continuous space using Lagrange polynomials [39,40]. The radial integrations are thereby reduced to sums over the values at the given radial grid points times a weighting factor. The remaining k integration is handled numerically, using Gauss-Legendre and Gauss-Laguerre quadrature. This procedure is performed for several partial-wave terms, the maximum number of l depending on the convergence properties of the given contribution. Finally, we extrapolate to $l\rightarrow\infty$.

B. Vertex and binding energy corrections

The vertex and the binding terms, which are shown in Fig. 3, are both infrared divergent and ultraviolet charge divergent, but the divergences cancel between the two terms. The infrared divergences can explicitly be shown to cancel between these terms [41]. Furthermore, the ultraviolet charge divergences will also cancel due to the Ward identity. To formulate an unambiguous regularization, we expand the intermediate bound-electron propagators in Eqs. (28) and (29) into free-electron propagators interacting zero, one, or several times with the nuclear potential. After separating out and canceling the infrared divergences [28], the one-potential and many-potential terms are finite and can readily be calculated in coordinate space using basis-set procedures as discussed above. The zero-potential terms are grouped together and by the use of dimensional regularization the ultraviolet divergences can be identified and canceled. The finite remainder was evaluated in momentum space.

The calculation of the vertex and binding energy corrections are thus arranged as follows:

$$\Delta E_{\mathrm{SE}}^{\mathrm{VE+BE}}=\Delta E_{\mathrm{ZP}}^{\mathrm{VE},p}+\Delta E_{\mathrm{ZP}}^{\mathrm{BE},p}+\Delta E_{\mathrm{HO}}^{\mathrm{VE+BE},x}$$
$$=\Delta E_{\mathrm{ZP}}^{\mathrm{VE+BE},p}+\Delta E_{\mathrm{HO}}^{\mathrm{VE+BE},x}, \tag{48}$$

where p and x again indicate momentum and coordinate space, respectively.

1. Zero-potential terms

The energy contribution from the zero-potential terms is given by

$$\Delta E_{\mathrm{ZP}}^{\mathrm{VE+BE},p}=\langle a|e\mathbf{\Lambda}(p,p')\cdot\mathbf{A}(\mathbf{p},\mathbf{p}')|a\rangle$$
$$+\Delta E^1\langle a|\frac{\partial}{\partial E}\Sigma(p)|a\rangle, \tag{49}$$

where ΔE^1 is the first-order hyperfine splitting and where $\mathbf{\Lambda}(p,p')$ and $(\partial/\partial E)\Sigma(p)$ are given by Eqs. (35) and (33), respectively. It is here implicitly understood that the canceling ultraviolet divergence Δ is omitted in the two parts.

The binding energy correction, $\Delta E_{\mathrm{ZP}}^{\mathrm{BE},p}$, has the same integral structure as the zero-potential part of the wave-function correction and it is evaluated in the same manner.

To compute the energy shift induced by the vertex correction one has to evaluate the following integral:

$$\Delta E_{\mathrm{ZP}}^{\mathrm{VE},p}=\frac{-ie}{(2\pi)^3}\int d^3\mathbf{p}d^3\mathbf{p}'\Psi_{Fm_F}^{\dagger}(\mathbf{p})\gamma_0[\boldsymbol{\gamma}f_1(p,p',\cos\vartheta)+\not{p}\mathbf{p}f_2(p,p',\cos\vartheta)+\not{p}\mathbf{p}'f_3(p,p',\cos\vartheta)+\not{p}'\mathbf{p}f_4(p,p',\cos\vartheta)$$
$$+\not{p}'\mathbf{p}'f_5(p,p',\cos\vartheta)+\not{p}\boldsymbol{\gamma}\not{p}'f_6(p,p',\cos\vartheta)+\mathbf{p}f_7(p,p',\cos\vartheta)+\mathbf{p}'f_8(p,p',\cos\vartheta)]\frac{\boldsymbol{\mu}\times(\mathbf{p}-\mathbf{p}')}{(\mathbf{p}-\mathbf{p}')^2}\Psi_{Fm_F}(\mathbf{p}'), \tag{50}$$

where the f_i functions are abbreviations for the coefficient functions of the vector part of Eq. (35). Due to the vector structure of this expression, we cannot reduce the angular part to some simple dependence on the intermediate angle as was done for the zeroth component of the vertex function. By defining the functions

$$V_i(p,p',\cos\vartheta)=\frac{f_i(p,p',\cos\vartheta)}{(\mathbf{p}-\mathbf{p}')^2}, \tag{51}$$

and expanding those according to Eq. (16), the angular dependencies can be separated. The angular integrations can thereby be performed analytically by using angular diagram techniques [35]. The final expression then contains the expansion integral Eq. (17) and the radial integrals over p and p', which are performed numerically.

2. One- and many-potential parts

The remaining contribution beyond the zero-potential part of the vertex diagram is convergent and can be calculated in coordinate space using the following expression:

$$\Delta E_{\mathrm{HO}}^{\mathrm{VE},x}=-\frac{\alpha}{\pi}\sum_{l=0}^{\infty}(2l+1)\int kdk\Bigg\{\sum_{m,n}\frac{\langle a|\alpha_\mu j_l(kr_3)\mathbf{C}^l|m\rangle\langle m|e\boldsymbol{\alpha}\cdot\mathbf{A}(\mathbf{r}_2)|n\rangle\langle n|j_l(kr_1)\mathbf{C}^l\alpha^\mu|a\rangle}{[E_a-E_m-\mathrm{sgn}(E_m)k][E_a-E_n-\mathrm{sgn}(E_n)k]}F$$
$$-\sum_{p,q}\frac{\langle a|\alpha_\mu j_l(kr_3)\mathbf{C}^l|p\rangle\langle p|e\boldsymbol{\alpha}\cdot\mathbf{A}(\mathbf{r}_2)|q\rangle\langle q|j_l(kr_1)\mathbf{C}^l\alpha^\mu|a\rangle}{[E_a-E_p-\mathrm{sgn}(E_p)k][E_a-E_q-\mathrm{sgn}(E_q)k]}F\Bigg\}, \tag{52}$$

where $|m\rangle,|n\rangle$ denotes bound-electron states and $|p\rangle,|q\rangle$ denotes free-electron states. Similarly, the higher-order binding corrections can be expressed as

$$\Delta E_{\mathrm{HO}}^{\mathrm{BE},x}=\frac{\alpha}{\pi}\sum_{l=0}^{\infty}(2l+1)\int kdk\Bigg\{\langle a|e\boldsymbol{\alpha}\cdot\mathbf{A}(\mathbf{r})|a\rangle\sum_{m}\frac{\langle a|\alpha_\mu j_l(kr_2)\mathbf{C}^l|m\rangle\langle m|j_l(kr_1)\mathbf{C}^l\alpha^\mu|a\rangle}{[E_a-E_m-\mathrm{sgn}(E_m)k]^2}$$
$$-\langle a|e\boldsymbol{\alpha}\cdot\mathbf{A}(\mathbf{r})|a\rangle\sum_{p}\frac{\langle a|\alpha_\mu j_l(kr_2)\mathbf{C}^l|p\rangle\langle p|j_l(kr_1)\mathbf{C}^l\alpha^\mu|a\rangle}{[E_a-E_p-\mathrm{sgn}(E_p)k]^2}\Bigg\}, \tag{53}$$

where $|m\rangle$ denotes bound-electron states and $|p\rangle$ denotes free-electron states. The evaluation scheme for these two contributions is discussed in the wave-function many-potential part.

IV. THE VACUUM-POLARIZATION CORRECTIONS

There are two different one-photon vacuum polarization diagrams that contribute to the hyperfine structure, see Figs. 1(b) and 1(c). The first is called the electric-loop correction (EL) since the polarization loop connects with the electrical potential of the nucleus. In the second diagram the loop connects with the nuclear magnetic vector potential and it is therefore called the magnetic-loop correction (ML). In the language of the self-energy corrections the EL part can be viewed as a wave-function modification and the ML part as a propagator modification. There is no binding energy term since the first-order vacuum polarization is independent of the reference energy E_a.

We have further considered the vacuum polarization correction to the measured nuclear magnetic moment. The Feynman diagram for this correction is shown in Fig. 4. This contribution contains a divergence due to the singular $1/r^2$ dependence of the point-dipole hyperfine potential. The divergence is also present in the Wichmann-Kroll part of the ML correction, and by combining the two effects we can eliminate the divergence and obtain a finite contribution. It should be pointed out that it is the unphysical nature of the nonrecoil point-dipole model that causes this divergence and it is not present when considering an extended nuclear magnetization model.

A. The electric-loop correction

The contribution from the electric-loop correction is given by

$$\Delta E_{\mathrm{VP}}^{\mathrm{EL}}=\sum_{t}\frac{\langle a|V_{\mathrm{VP}}|t\rangle\langle t|e\boldsymbol{\alpha}\cdot\mathbf{A}_{\mathrm{HFS}}|a\rangle}{E_a-E_t}+\mathrm{c.c.},$$

with $E_t\neq E_a$. Here we have explicitly indicated the hyperfine potential $\mathbf{A}_{\mathrm{HFS}}$ to separate it from other vector potentials appearing later. The vacuum-polarization potential V_{VP} consists of the charge renormalized Uehling part (Ue) (one-potential term) [42] and the Wichmann-Kroll part (WK) (many-potential term) [43]. This contribution is readily evaluated using the techniques described in Ref. [44].

The electric-loop contribution can also be computed to all orders in V_{VP} by including the vacuum polarization potential when solving the Dirac equation. The wave functions obtained are then used when evaluating the first-order hyperfine splitting.

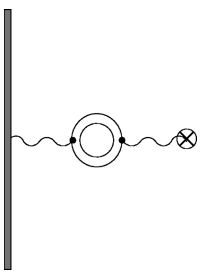

FIG. 4. Feynman diagram representing the vacuum polarization correction to the nuclear magnetic moment. The filled line indicates the nuclear wave function and the crossed circle represents the interaction with the external homogeneous magnetic field.

B. The magnetic-loop correction

For the magnetic-loop correction the expression reads

$$\Delta E_{\rm VP}^{\rm ML}=-\frac{4\alpha}{\pi}\sum_{l=0}^{\infty}(2l+1)\int dk\langle a|\alpha_\mu j_l(kr_1)\mathbf{C}^l|a\rangle \times\sum_n^+\sum_m^-\frac{\langle n|\alpha^\mu j_l(kr_2)\mathbf{C}^l|m\rangle\langle m|e\boldsymbol{\alpha}\cdot\mathbf{A}_{\rm HFS}|n\rangle}{E_n-E_m}, \tag{54}$$

where the different signs at the sum symbols indicate that the loop contains only virtual electron-positron pairs. This expression can also be written in the compact form

$$\Delta E_{\rm VP}^{\rm ML}=-2\sum_n^+\sum_m^-\frac{\langle n|e\boldsymbol{\alpha}\cdot\mathbf{A}_{1s}|m\rangle\langle m|e\boldsymbol{\alpha}\cdot\mathbf{A}_{\rm HFS}|n\rangle}{E_n-E_m}, \tag{55}$$

where we have defined the potential from the $1s$ electron as

$$e\mathbf{A}_{1s}(\mathbf{r})=-\frac{2\alpha}{\pi}\sum_{l=0}^{\infty}(2l+1)\mathbf{C}^l(\hat r)\int dk j_l(kr) \times\langle a|\boldsymbol{\alpha}j_l(kr')\mathbf{C}^l(\hat r')|a\rangle. \tag{56}$$

By expanding the loop propagators in the nuclear Coulomb potential one obtains a zero-potential term, two one-potential terms, and finally higher-order terms with two or more nuclear Coulomb interactions. Terms with an odd number of loop vertices will vanish due to Furry's theorem. This implies that only the terms with an even number of nuclear Coulomb interactions will survive in the expansion.

The zero-potential part represents the Uehling correction and is renormalized and calculated separately. We have computed the Uehling contribution in both coordinate and momentum space. In the momentum space calculation we evaluate the first-order splitting with the Uehling potential

$$\mathbf{A}^{\rm Ue}(\mathbf{q})=\Pi^{\rm ren}(\mathbf{q}^2)\mathbf{A}_{\rm HFS}(\mathbf{q}), \tag{57}$$

where $\Pi^{\rm ren}(\mathbf{q}^2)$ is the renormalized free-electron polarization function [45]. The corresponding expression for the energy contribution in coordinate space is given by [23]

$$\Delta E_{\rm VP}^{\rm ML\text{-}Ue}=-\frac{eg_I\mu_N}{4\pi}\frac{2}{3}[F_2(F_2+1)-F_1(F_1+1)] \times\left[2\frac{2}{3}\frac{\alpha}{\pi}\int_1^\infty dz\sqrt{1-\frac{1}{2z^2}}\left(1+\frac{1}{2z^2}\right)\frac{1}{z} \times\int_0^\infty r^2dr\frac{f(r)g(r)}{r^2}e^{-2mrz}[2mrz+1]\right], \tag{58}$$

and is straightforward to evaluate.

The higher-order terms in the expansion are together called the Wichmann-Kroll part and are evaluated by taking the difference between the unrenormalized bound- and free-loop expressions [28,44]. The first nonvanishing terms are the two-potential terms (light-by-light scattering), which contain a spurious gauge-dependent piece that has to be removed. This can be done by expanding the loop propagators in partial waves (κ) and restricting the expansion to a finite number of terms [46–48]. The Wichmann-Kroll contribution is given by the subtraction

$$\Delta E_{\rm VP}^{\rm ML\text{-}WK}=-2\left\{\sum_n^+\sum_m^-\frac{\langle n|e\boldsymbol{\alpha}\cdot\mathbf{A}_{1s}|m\rangle\langle m|e\boldsymbol{\alpha}\cdot\mathbf{A}_{\rm HFS}|n\rangle}{E_n-E_m} -\sum_p^+\sum_q^-\frac{\langle p|e\boldsymbol{\alpha}\cdot\mathbf{A}_{1s}|q\rangle\langle q|e\boldsymbol{\alpha}\cdot\mathbf{A}_{\rm HFS}|p\rangle}{E_p-E_q}\right\}, \tag{59}$$

where $|n\rangle,|m\rangle$ denote bound intermediate states and $|p\rangle,|q\rangle$ denote the corresponding free states. The singular $1/r^2$ dependence of the point-dipole hyperfine potential leads to divergent integrals in this expression. With an extended magnetization the singularity is removed and the correction is finite. The divergence of the Wichmann-Kroll part is present also in the correction to the measured nuclear magnetic moment, and we can cancel the divergence by combining the two effects, as will be shown in the following subsection.

C. Vacuum polarization correction to the nuclear magnetic moment

Similarly as for the electron g factor [49], the Wichmann-Kroll effect gives a correction to the measured nuclear magnetic moment. This correction, as well as the correction $\Delta E_{\rm VP}^{\rm ML\text{-}WK}$ given above, diverges in the point-dipole model.

TABLE I. The low-Z self-energy corrections given in terms of the function $F_{\rm SE}^{(2)}(Z\alpha)$. As a comparison, the values of the $(Z\alpha)$ expansion and the results of Ref. [8] are also given.

Z	$E_{\rm SE}^{\rm WF}$	$E_{\rm ZP}^{{\rm BE},p}$	$E_{\rm ZP}^{{\rm VE},p}$	$E_{\rm HO}^{{\rm VE+BE},x}$	Total SE	$F(Z\alpha)$	Ref. [8]
1	−0.0110	7.7895	−5.0795	−2.2610	0.4380(1)	0.438 11	0.438 08
3	−0.0519	5.6036	−3.1124	−2.1318	0.3075(1)	0.307 73	0.307 59
5	−0.1049	4.5996	−2.3008	−2.0197	0.1741(1)	0.174 75	0.174 05
7	−0.1651	3.9487	−1.8226	−1.9215	0.0395(1)	0.041 54	0.039 50
10	−0.2639	3.2744	−1.3779	−1.7954	−0.1628(1)	−0.156 57	−0.162 83

TABLE II. The self-energy corrections for the high-Z region given in terms of $F_{\mathrm{SE}}^{(2)}(Z\alpha)$. In the last two columns the results of Refs. [7,10] are given as a comparison. These values are scaled to our units by using the first-order values (from a uniform nuclear charge distribution) given in Table V.

Z	$E_{\mathrm{SE}}^{\mathrm{WF}}$	$E_{\mathrm{ZP}}^{\mathrm{BE},p}$	$E_{\mathrm{ZP}}^{\mathrm{VE},p}$	$E_{\mathrm{HO}}^{\mathrm{VE+BE},x}$	Total SE	Ref. [10]	Ref. [7]
67	−3.8506	0.3309	−0.7515	−1.3894	−5.6605	−5.662	−5.6625
75	−5.0639	0.1818	−0.9484	−1.5295	−7.3599	−7.362	
82	−6.5211	0.0508	−1.1896	−1.7085	−9.3683		
83	−6.7694	0.0316	−1.2307	−1.7393	−9.7078	−9.707	−9.7111

Cutting off the small distances leads to a logarithmic divergence in the cutoff radius. This logarithmic behavior is well known from calculations of the anomalous magnetic moment of the muon [50–52], and also from earlier treatments of the nuclear magnetic moment correction [53,54].

In an external homogeneous magnetic field **B**, described by the vector potential $\mathbf{A}_{\mathrm{mag}}=-(\mathbf{r}\times\mathbf{B})/2$, the correction to the nuclear magnetic moment can be written as

$$\Delta\boldsymbol{\mu}_{\mathrm{WK}}=-\frac{2\boldsymbol{\mu}_{\mathrm{bare}}}{g_I m_I \mu_N |\mathbf{B}|}\left\{\sum_n^{+}\sum_m^{-}\frac{\langle n|e\boldsymbol{\alpha}\cdot\mathbf{A}_{\mathrm{mag}}|m\rangle\langle m|e\boldsymbol{\alpha}\cdot\mathbf{A}_{\mathrm{HFS}}|n\rangle}{E_n-E_m}-\sum_p^{+}\sum_q^{-}\frac{\langle p|e\boldsymbol{\alpha}\cdot\mathbf{A}_{\mathrm{mag}}|q\rangle\langle q|e\boldsymbol{\alpha}\cdot\mathbf{A}_{\mathrm{HFS}}|p\rangle}{E_p-E_q}\right\}, \tag{60}$$

where $\boldsymbol{\mu}_{\mathrm{bare}}$ is the bare magnetic moment, i.e., the unperturbed nuclear magnetic moment. This correction is included in the measured nuclear magnetic moment

$$\boldsymbol{\mu}_{\mathrm{expt.}}=\boldsymbol{\mu}_{\mathrm{bare}}+\Delta\boldsymbol{\mu}_{\mathrm{WK}}=\boldsymbol{\mu}_{\mathrm{bare}}(1+\boldsymbol{\epsilon}), \tag{61}$$

and cannot be separated out. In order to avoid double counting, the bare magnetic moment should be used when calculating the hyperfine structure. Specifically, one should correct for the shift in the magnetic moment when calculating the first-order hyperfine splitting,

$$\Delta E_{\mathrm{HFS}}^{1,\mathrm{bare}}=\Delta E_{\mathrm{HFS}}^{1,\mathrm{expt.}}(1-\boldsymbol{\epsilon}). \tag{62}$$

This opens the possibility to ''renormalize'' the point-dipole divergency in the corrections Eqs. (59) and (62). We therefore employ the calculation scheme

$$\begin{aligned}\Delta E_{\mathrm{VP}}^{\mathrm{ML\text{-}WK\text{-}ren}}&=\Delta E_{\mathrm{VP}}^{\mathrm{ML\text{-}WK}}-\Delta E_{\mathrm{HFS}}^{1,\mathrm{expt.}}\times\boldsymbol{\epsilon}\\&=-2\left\{\sum_n^{+}\sum_m^{-}\frac{\langle n|e\boldsymbol{\alpha}\cdot(\mathbf{A}_{1s}-\beta\mathbf{A}_{\mathrm{mag}})|m\rangle\langle m|e\boldsymbol{\alpha}\cdot\mathbf{A}_{\mathrm{HFS}}|n\rangle}{E_n-E_m}-\sum_p^{+}\sum_q^{-}\frac{\langle p|e\boldsymbol{\alpha}\cdot(\mathbf{A}_{1s}-\beta\mathbf{A}_{\mathrm{mag}})|q\rangle\langle q|e\boldsymbol{\alpha}\cdot\mathbf{A}_{\mathrm{HFS}}|p\rangle}{E_p-E_q}\right\},\end{aligned} \tag{63}$$

where $\beta=\Delta E_{\mathrm{HFS}}^{1,\mathrm{expt.}}/(g_I m_I \mu_N|\mathbf{B}|)$. With this scheme the $1/r^2$ divergence is eliminated and we can obtain the combined effect of the Wichmann-Kroll correction to the hyperfine structure and to the nuclear magnetic moment. It should be pointed out that we take the effect of the corrected magnetic moment into account only in the first-order splitting, since it would lead to uncontrolled higher-order effects when applied to the QED corrections.

V. NUMERICAL RESULTS

Our results for the self-energy and vacuum-polarization corrections to the hyperfine structure can be divided into different categories. Low Z are considered in order to compare with the known part of the $(Z\alpha)$ expansion. The hyperfine structure for several high-Z ions has recently been measured and calculations for some of these systems are also presented here. In Tables I and II our SE results are given and the VP results are presented in Tables III and IV. We have further investigated how the SE and VP corrections are affected by using an extended nuclear magnetization for the high-Z systems and these results are displayed in Tables V and VI. Finally, we collect recent theoretical results for these high-Z ions and compare with experiment in Table VII.

All values, except those in Tables VI and VII, are pre-

TABLE III. The low-Z Uehling vacuum-polarization corrections given in terms of the function $F_{\mathrm{VP}}^{(2)}(Z\alpha)$. The results of the $(Z\alpha)$ expansions are given in columns three and five, and in the last column the total numerical value is collected.

Z	$E_{\mathrm{VP}}^{\mathrm{EL\text{-}Ue}}$	$F^{\mathrm{EL}}(Z\alpha)$	$E_{\mathrm{VP}}^{\mathrm{ML\text{-}Ue}}$	$F^{\mathrm{ML}}(Z\alpha)$	Total num.
1	0.008 769 1	0.008 768 7	0.008 557 8	0.008 556 6	0.017 327
3	0.027 112	0.027 067	0.025 487	0.025 455	0.052 599
5	0.046 414	0.046 194	0.042 257	0.042 109	0.088 670
7	0.066 671	0.066 043	0.058 960	0.058 558	0.125 631
10	0.098 955	0.097 033	0.084 072	0.082 908	0.183 028

TABLE IV. The vacuum polarization corrections given in terms of the function $F_{\rm VP}^{(2)}(Z\alpha)$. The $R_{\rm rms}$ values used for the nuclear electric charge distribution are given in the second column (fm). In columns three and four the EL and ML Uehling parts are displayed. The Wichmann-Kroll part of the EL diagram is given in column five followed by the ''renormalized'' ML Wichmann-Kroll contribution (from Table V).

Z	$R_{\rm rms}$	$E_{\rm VP}^{\rm EL\text{-}Ue}$	$E_{\rm VP}^{\rm ML\text{-}Ue}$	$E_{\rm VP}^{\rm EL\text{-}WK}$	$E_{\rm VP}^{\rm ML\text{-}WK\text{-}ren}$	Total VP
10	2.99	0.094 922	0.080 275	−0.000 054	−0.000 271	0.174 871
18	3.42	0.188 65	0.144 80	−0.000 35	−0.001 60	0.331 50
32	4.07	0.411 76	0.271 53	−0.002 18	−0.009 70	0.671 41
54	4.78	1.083 1	0.563 0	−0.014 6	−0.060 9	1.570 7
67	5.21	1.900	0.847	−0.037	−0.147	2.562
75	5.351	2.742	1.102	−0.063	−0.249	3.533
82	5.497	3.843	1.404	−0.102	−0.391	4.754
83	5.519	4.038	1.455	−0.109	−0.418	4.967

sented in terms of the function F, which is defined through

$$\Delta E = \Delta E_F \frac{\alpha}{\pi} F, \tag{64}$$

where ΔE_F is the nonrelativistic, point-nucleus first-order hyperfine splitting. Note that this definition differs from the one used in a previous paper [6], where the relativistic and extended nuclear charge effects were incorporated in the first-order value.

To make a consistent comparison with the $(Z\alpha)$ expansions we have performed the low-Z calculations (Tables I and III) using a point nuclear-charge model. All other QED corrections are evaluated with a uniform nuclear-charge distribution with $R_{\rm rms}$ values as given in Table IV.

A. Self-energy

The self-energy corrections are presented in Tables I and II for the low- and high-Z regions, respectively. The total SE value is composed of various parts as described in the text. Our values agree well with those of [8] and the discrepancies between their values and values from an earlier calculation presented in [6] are now absent. The earlier deviation was originating from a small computational error in our evaluation of the term $E_{\rm ZP}^{{\rm VE},p}$. The low-Z values presented in [8] are still an order of magnitude more accurate than ours, so we cannot add more information about the $(Z\alpha)$-expansion comparison than was done in their paper. The limitations in our computation come mainly from the $E_{\rm HO}^{{\rm VE+BE},x}$ term where a large number of partial-wave terms have to be calculated in order to decrease the extrapolation error. We should be able to increase our accuracy substantially if we could evaluate the slowly converging one-Coulomb potential vertex term semianalytically as was successfully accomplished in the g_j-factor case [49]. It would then also be necessary to improve the accuracy in the computation of the $E_{\rm SE}^{\rm WF}$ term.

B. Vacuum polarization

The results for the vacuum polarization corrections are presented in Tables III and IV. The low-Z values displayed in Table III are the results in the Uehling approximation since the $(Z\alpha)$ expansion is evaluated in this approximation. The $(Z\alpha)$ expansion for the VP corrections can be separated in two parts [55], corresponding to the electric [Fig. 1(b)] and magnetic [Fig. 1(c)] diagrams

$$\Delta E_{\rm VP}^{(2)} = \Delta E_F \frac{\alpha}{\pi} (F_{\rm VP\text{-}EL}^{(2)} + F_{\rm VP\text{-}ML}^{(2)}), \tag{65}$$

where

TABLE V. The constituents and the ''renormalization'' of the magnetic loop Wichmann-Kroll correction using different magnetization models. For the point-dipole model only the combined effect can be evaluated directly. All values (except ϵ) are given in units of $(\alpha/\pi)E_F$ and the number in parentheses indicates the power of ten.

Z	Model	$E_{\rm VP}^{\rm ML\text{-}WK}$	ϵ	$\Delta E_{\rm HFS}^{1,\rm expt.}$	$\Delta E_{\rm VP}^{\rm ML\text{-}WK\text{-}ren}$
10	pnt			433.48	−0.000 271
	$n=0$	0.009 670	2.292(−5)	433.30	−0.000 261
18	pnt			440.81	−0.001 60
	$n=0$	0.029 78	7.110(−5)	440.40	−0.001 53
32	pnt			465.52	−0.009 70
	$n=0$	0.089 89	2.133(−4)	464.46	−0.009 16
54	pnt			546.18	−0.060 9
	$n=0$	0.2638	5.898(−4)	542.69	−0.056 2
67	pnt			632.17	−0.147
	$n=0$	0.4304	9.021(−4)	625.14	−0.134
	$n=2$	0.4203	8.841(−4)	623.90	−0.131
75	pnt			709.08	−0.249
	$n=0$	0.5754	1.143(−3)	698.36	−0.223
	$n=2$	0.5614	1.120(−3)	696.45	−0.219
82	pnt			798.04	−0.391
	$n=0$	0.7351	1.382(−3)	782.20	−0.346
	$n=2$	0.7163	1.353(−3)	779.38	−0.338
83	pnt			812.86	−0.418
	$n=0$	0.7614	1.419(−3)	796.05	−0.368
	$n=2$	0.7410	1.388(−3)	793.09	−0.360
	DPM	0.8037	1.483(−3)	802.46	−0.386

TABLE VI. The first-order splitting (using a Fermi nuclear charge distribution) and the QED values for some different magnetization models. The values for Pb are computed using the value $0.592\,583(9)\mu_N$ [57] for the nuclear magnetic moment. Note that the finite magnetization effect on the QED values nearly vanishes due to cancellations between the vacuum polarization and the self-energy parts. All values are given in eV.

Ion	Model	$\Delta E^1_{\rm Fermi}$	VP	SE	VP+SE
$^{165}Ho^{66+}$	pnt	2.1954	0.008 90	−0.019 65	−0.010 76
	$n=0$	2.1740	0.008 53	−0.019 23	−0.010 70
	$n=2$	2.1702	0.008 47	−0.019 16	−0.010 69
$^{185}Re^{74+}$	pnt	2.7976	0.013 93	−0.029 02	−0.015 09
	$n=0$	2.7594	0.013 24	−0.028 22	−0.014 98
	$n=2$	2.7526	0.013 12	−0.028 08	−0.014 95
$^{207}Pb^{81+}$	pnt	1.2755	0.007 59	−0.014 96	−0.007 37
	$n=0$	1.2526	0.007 15	−0.014 44	−0.007 29
	$n=2$	1.2486	0.007 07	−0.014 34	−0.007 27
$^{209}Bi^{82+}$	pnt	5.1911	0.031 70	−0.061 96	−0.030 26
	$n=0$	5.0914	0.029 81	−0.059 71	−0.029 90
	$n=2$	5.0739	0.029 49	−0.059 32	−0.029 83
	DPM	5.1233	0.030 52	−0.060 56	−0.030 04

$$F^{(2)}_{\rm VP\text{-}EL}=\frac{3}{8}\pi(Z\alpha)-\frac{8}{15}\ln(Z\alpha)(Z\alpha)^2+\left(\frac{214}{225}-\frac{8}{15}\ln 2\right)\times(Z\alpha)^2-\frac{\pi}{6}\ln(Z\alpha)(Z\alpha)^3 \quad (66)$$

and

$$F^{(2)}_{\rm VP\text{-}ML}=\frac{3}{8}\pi(Z\alpha)-\frac{4}{5}(Z\alpha)^2-\frac{3}{8}\pi\ln(Z\alpha)(Z\alpha)^3. \quad (67)$$

As can be seen from Table III, the agreement between the numerical results and the $(Z\alpha)$ expansion is very good for low Z.

In Table IV the VP corrections for $Z\geqslant 10$ are presented. The $R_{\rm rms}$ values used for the nuclear electric charge distribution are given in the second column. The total VP correction consists of the electric and magnetic Uehling parts (columns three and four), the electric Wichmann-Kroll part (column five), and finally the ''renormalized'' Wichmann-Kroll correction to the magnetic loop diagram (column six). Here only the total magnetic loop WK correction is listed since the individual parts cannot be directly calculated using a point nuclear magnetization. The breakup and structure of this correction is discussed further in the next subsection.

C. Effects of extended nuclear magnetization on QED

The Wichmann-Kroll corrections to the magnetic loop diagram ($E^{\rm ML\text{-}WK}_{\rm VP}$), to the nuclear magnetic moment (ϵ), and the combined effect of those ($E^{\rm ML\text{-}WK\text{-}ren}_{\rm VP}$) are presented in Table V. For each Z the calculations are performed using different models for the nuclear magnetization distribution. Here and later on we will use the notation ''pnt'' for the point-dipole model, ''$n=0$'' and ''$n=2$'' refer to the model of Ref. [13] [see Eq. (21)], and ''DPM'' stands for the dynamical proton model [16]. We have implemented the DPM using the same parameters as in Ref. [16] and scaled the interaction to achieve the experimental nuclear magnetic moment.

The individual WK corrections diverge in the point-dipole model and can only be calculated with an extended nuclear magnetization. Their combined contribution is, however, free from the divergent part and can thus be evaluated also for the point-dipole model. It is interesting to note the different Z scaling laws for the constituents and the combined value. From the table one can see that $E^{\rm ML\text{-}WK}_{\rm VP}$ and $\epsilon E^{1,\,\rm expt.}_{\rm HFS}$ scale with approximately the same power of Z, i.e., nearly quadratic in these units. The combined value scales faster ($\approx Z^3$) and exhibits almost exactly the expected extra two powers of Z in comparison with the Uehling part ($E^{\rm ML\text{-}Ue}_{\rm VP}$ in Table IV).

The Wichmann-Kroll correction to the nuclear magnetic moment has earlier been considered by Milstein and Yelkhovsky [53,54]. The point nucleus model was used

TABLE VII. The total theoretical values are collected and compared with recent experimental results. The QED values are taken from the $n=2$ magnetization model in Table VI. For Pb we give the results using two different experimental values for the magnetic moment, $0.592\,583(9)\mu_N$ [57] in the first row and $0.582\,19(2)\mu_N$ [57] in the second row. All values are given in eV.

Ion	$\Delta E^1_{\rm Fermi}$	BW	QED	Total theory	Experiment
$^{165}Ho^{66+}$	2.1954(5)(27)	−0.0195(59)[a]	−0.0107	2.1652(65)	2.1645(6) [b]
$^{185}Re^{74+}$	2.7976(15)(3)	−0.034(10) [a]	−0.0150	2.749(10)	2.719(2) [c]
$^{207}Pb^{81+}$	1.2755(1)(0)	−0.0534(53)[a]	−0.0073	1.2148(53)	1.2159(2) [d]
	1.2531(1)(0)	−0.0525(53)[a]	−0.0071	1.1934(53)	
$^{209}Bi^{82+}$	5.1911(7)(3)	−0.107(7) [e]	−0.0298	5.0542(70)	5.0840(8) [f]
		−0.061(27) [a]	−0.0298	5.1002(270)	
		−0.0678 [g]	−0.0300[g]	5.0933(8) [g]	

[a]Taken from Refs. [9,56].
[b]Reference [3].
[c]Reference [4].
[d]Reference [5].
[e]Taken from Ref. [15].
[f]Reference [2].
[g]Results using the dynamical proton model (DPM).

(both for the charge and the magnetization) and the divergency was regularized by introducing a small distance cutoff (R_c). They further set the electron mass to zero and imposed therefore also a large distance cutoff at the electron Compton wavelength ($\lambda\!\!\!^{-}_e$). With these conditions they obtained the logarithmic term

$$\epsilon = \frac{2\alpha}{3\pi}\ln\left(\frac{\lambda\!\!\!^{-}_e}{R_c}\right)F(Z\alpha). \tag{68}$$

The function $F(Z\alpha)$ was evaluated to all orders in $(Z\alpha)$ and was shown to have a quadratic low-Z dependence,

$$F(Z\alpha)\approx(Z\alpha)^2[1+0.657(Z\alpha)^2]. \tag{69}$$

To check the consistency with our complete Wichmann-Kroll calculations, we have, in addition to the full calculation, performed this cutoff regularization procedure. Whereas Milstein and Yelkhovsky considered only the logarithmic part in their work, we obtain in our calculation also nonsingular terms beyond the logarithm. These terms are significant and lead to a rather large deviation ($\approx 50\%$) between the results when using experimental nuclear radii as the cutoff. Decreasing the radius will enhance the logarithmic term and the agreement between the results becomes increasingly better.

To compare the two different calculations we performed fittings of our numerical values to the expression

$$\epsilon = A(R_c, Z\alpha) + B(Z\alpha)\ln\left(\frac{\lambda\!\!\!^{-}_e}{R_c}\right), \tag{70}$$

for different values of Z and R_c. With such fittings we could verify the result of Milstein and Yelkhovsky with an accuracy of about 2%. For low Z ($Z \leqslant 18$), our result can be expressed in the form

$$\epsilon = \frac{\alpha}{\pi}(Z\alpha)^2\left[\frac{2}{3}\ln\left(\frac{\lambda\!\!\!^{-}_e}{R_c}\right) + C\right], \tag{71}$$

with $C \approx -1.2$.

Table VI shows the effect of using an extended nuclear magnetization on the QED and the first-order values. Note that the first-order splitting is here calculated using a two-parameter Fermi model for the nuclear charge distribution. The Fermi model parameters and the nuclear magnetic moments used are displayed in Table VIII.

From Table VI it is seen that the effect of an extended nuclear magnetization is very small for the total QED values. This is due to a large cancellation between the VP and SE corrections. This implies that not only the absolute effect but also the relative effect is smaller for QED than for the first-order value. The total effect of an extended nuclear magnetization on the hyperfine splitting is thus almost completely determined by the effect on the first-order value. We have also investigated the sensibility of the QED corrections due to variations of the nuclear charge radius. Also in this case there is a large cancellation between the VP and SE parts and the resulting uncertainty is found to be unimportant in comparison to the effect of varying the magnetization distribution. The conclusion is thus that the uncertainty due to the nuclear charge and magnetic distribution is completely dominated by the effects on the first-order splitting.

TABLE VIII. Table of the nuclear parameters used in this work. The Fermi parameter a is related to the skin thickness (t) via the relation $t = 4a\ln 3$.

Ion	a (fm)	$R_{\rm rms}$ (fm)	$\mu(\mu_N)$
$^{165}_{67}$Ho	0.57(1) [a]	5.21(3) [a]	4.132(5) [b]
$^{185}_{75}$Re	0.524(20) [c]	5.351(50) [d]	3.1871(3) [e]
$^{207}_{82}$Pb	0.546(10) [a]	5.497(2) [a]	0.592 583(9) [e]
$^{209}_{83}$Bi	0.468(39) [a]	5.519(4) [a]	4.1106(2) [e]

[a]From Ref. [11].
[b]From Refs. [3,58,59].
[c]Default skin thickness.
[d]From Ref. [60].
[e]From Ref. [57].

Comparing the first-order values displayed in Table VI and the Bohr-Weisskopf values of Table VII, it can be deduced that the Bohr-Weisskopf effect for the $n=0$ and $n=2$ models is in fair agreement with earlier published results [9,15] for Ho, Re, and Bi. For Pb there is, however, a large deviation between the result given in Ref. [9] (-53.4 meV) and the values presented here (-22.9 meV for $n=0$ and -26.9 meV for $n=2$), indicating a magnetization located far out from the nuclear center. For that reason we have also calculated the QED values for Pb assuming that the magnetization is located at the nuclear surface ($n=\infty$). We obtain then 6.91 meV for the VP correction and -14.14 meV for the SE correction. This yields a total QED correction of -7.23 meV, which corresponds only to a 2% difference between the shell model and the point-dipole model.

D. Comparison with experiment

In order to obtain total theoretical values we have also collected different values of the Bohr-Weisskopf effect from the literature. These are added to our first-order hyperfine energies (using point nuclear magnetic moment) together with the QED corrections in Table VII. Finally, the total results are compared with experiment.

For Pb we give results for two different experimental values of the nuclear magnetic moment. In the first row we have used the value $0.592\,583(9)\mu_N$ [57], which is also the one used in Table VI. This value was obtained using NMR in a liquid solution and the chemical shift correction is not taken into account. The results in the second row are obtained by using the value $0.582\,19(2)\mu_N$ [57] from an optical pumping measurement.

The first-order splitting has been calculated using the two-parameter Fermi model for the nuclear charge distribution, with the parameters tabulated in Table VIII. There are two different error bars assigned to the first-order value. The first is due to the experimental uncertainties in the $R_{\rm rms}$ and skin thickness values and the second error is obtained from the uncertainty in the magnetic moment (see Table VIII).

The Bohr-Weisskopf values are taken from Refs. [9,56]. For Bi we also give results using the Bohr-Weisskopf value of Ref. [15] and results using the DPM (last row). The Bohr-

Weisskopf effect is difficult to calculate with high accuracy since this requires a detailed knowledge of the nuclear structure. The uncertainties assigned to these values should therefore be considered only as the order of magnitude of the expected error [9].

The QED values are taken from the $n=2$ magnetization model in Table VI. Adding the first-order splitting, the Bohr-Weisskopf effect, and the QED value we obtain the total theoretical hyperfine splitting displayed in column five. The agreement between theory and experiment is fair even though the uncertainties associated with the Bohr-Weisskopf effect and the nuclear magnetic moment restrict the test of the QED corrections.

VI. CONCLUSIONS

We have considered the influence of the extended nuclear charge and magnetic moment distributions on the one-photon QED corrections to the 1*s* hyperfine structure. This includes the complete evaluation of the vacuum polarization corrections, i.e., also the Wichmann-Kroll effect on both the magnetic-loop and electric-loop diagrams.

In the point magnetic moment case, we find for the self-energy correction good agreement with other recently performed calculations [7–9]. Furthermore, when using different extended magnetization distributions we find only small variations in the QED values. Thus, we conclude that the totally dominating theoretical uncertainty lies in the first-order hyperfine splitting value. These uncertainties are due to the lack of detailed knowledge about the magnetization distribution, and also the experimental values of the magnetic dipole moments are not fully reliable. The moments that are measured in a chemical solution may suffer from chemical shifts, but this source of error could be eliminated using a more accurate experimental method.

ACKNOWLEDGMENTS

The authors are very grateful to W. Greiner, M. G. H. Gustavsson, S. G. Karshenboim, A. I. Milstein, A. Schäfer, V. M. Shabaev, and A. S. Yelkhovsky for enlightening discussions. We want to thank V. M. Shabaev, in particular, for the suggestion to treat the magnetic-loop Wichmann-Kroll part together with the VP correction to the measured nuclear-magnetic moment. S.M.S. wants to thank the DAAD for financial support. The work of H.P. and I.L. was supported by the Alexander von Humboldt Stiftung.

[1] W. Pauli, Naturwissenschaften **12**, 741 (1924).
[2] I. Klaft, S. Borneis, T. Engel, B. Fricke, R. Grieser, G. Huber, T. Kühl, D. Marx, R. Neumann, S. Schröder, P. Seelig, and L. Völker, Phys. Rev. Lett. **73**, 2425 (1994).
[3] J. R. Crespo Lopez-Urrutia, P. Beiersdorfer, D. Savin, and K. Widmann, Phys. Rev. Lett. **77**, 826 (1996).
[4] J. R. Crespo-Lopez-Urrutia, P. Beiersdorfer, K. Widmann, B. B. Birkett, A.-M. Mårtensson-Pendrill, and M. G. H. Gustavsson, Phys. Rev. A **57**, 879 (1998).
[5] P. Seelig *et al.* (unpublished).
[6] H. Persson, S. M. Schneider, G. Soff, W. Greiner, and I. Lindgren, Phys. Rev. Lett. **76**, 1433 (1996).
[7] S. A. Blundell, K. T. Cheng, and J. Sapirstein, Phys. Rev. A **55**, 1857 (1997).
[8] S. A. Blundell, K. T. Cheng, and J. Sapirstein, Phys. Rev. Lett. **78**, 4914 (1997).
[9] V. M. Shabaev, M. Tomaselli, T. Kühl, A. N. Artemyev, and V. A. Yerokhin, Phys. Rev. A **56**, 252 (1997).
[10] V. M. Shabaev, M. B. Shabaeva, I. I. Tupitsyn, V. A. Yerokhin, A. N. Artemyev, T. Kühl, M. Tomaselli, and O. M. Zherebtsov, Phys. Rev. A **57**, 149 (1998).
[11] H. de Vries, C. W. de Jager, and C. de Vries, At. Data Nucl. Data Tables **36**, 495 (1987).
[12] A. Bohr and V. F. Weisskopf, Phys. Rev. **77**, 94 (1950).
[13] M. Finkbeiner, B. Fricke, and T. Kühl, Phys. Lett. A **176**, 113 (1993).
[14] S. M. Schneider, J. Schnaffner, G. Soff, and W. Greiner, J. Phys. B **26**, L581 (1993).
[15] M. Tomaselli, S. M. Schneider, E. Kankeleit, and T. Kühl, Phys. Rev. C **51**, 2989 (1995).
[16] L. N. Labzowsky, W. R. Johnson, S. M. Schneider, and G. Soff, Phys. Rev. A **51**, 4597 (1995).
[17] J. Schwinger, Phys. Rev. **73**, 416 (1948).
[18] N. M. Kroll and F. Pollock, Phys. Rev. **85**, 876 (1952).
[19] R. Karplus and A. Klein, Phys. Rev. **85**, 927 (1952).
[20] D. E. Zwanziger, Phys. Rev. **121**, 1128 (1961).
[21] S. J. Brodsky and G. W. Erickson, Phys. Rev. **148**, 26 (1966).
[22] J. R. Sapirstein, Phys. Rev. Lett. **51**, 985 (1983).
[23] S. M. Schneider, G. Soff, and W. Greiner, Phys. Rev. A **50**, 118 (1994).
[24] S. G. Karshenboim, Z. Phys. D **36**, 11 (1996).
[25] K. Pachucki, Phys. Rev. A **54**, 1994 (1996).
[26] M. Nio and T. Kinoshita, Phys. Rev. D **55**, 7267 (1997).
[27] E. Fermi, Z. Phys. **60**, 320 (1930).
[28] H. Persson, S. Salomonson, P. Sunnergren, and I. Lindgren, Phys. Rev. Lett. **76**, 204 (1996).
[29] M. Gell-Mann and F. Low, Phys. Rev. **84**, 350 (1951).
[30] J. Sucher, Phys. Rev. **107**, 1448 (1957).
[31] P. Indelicato and P. J. Mohr, Theor. Chim. Acta **80**, 207 (1991).
[32] N. J. Snyderman, Ann. Phys. (N.Y.) **211**, 43 (1991).
[33] S. A. Blundell and N. J. Snyderman, Phys. Rev. A **44**, R1427 (1991).
[34] K. T. Cheng, W. R. Johnson, and J. Sapirstein, Phys. Rev. A **47**, 1817 (1993).
[35] I. Lindgren and J. Morrison, *Atomic Many-Body Theory* (Springer, Berlin, 1982).
[36] I. Lindgren, H. Persson, S. Salomonson, and L. Labzowsky, Phys. Rev. A **51**, 1167 (1995).
[37] S. M. Schneider, doctoral thesis, Johann Wolfgang Goethe-Universität, Frakfurt am Main, 1995 (unpublished).
[38] S. Salomonson and P. Öster, Phys. Rev. A **40**, 5548 (1989).
[39] H. Persson, I. Lindgren, and S. Salomonson, Phys. Scr. **T46**, 125 (1993).
[40] H. Persson, doctoral thesis, Göteborg University, Göteborg, 1993 (unpublished).

[41] P. Sunnergren, licenciate thesis, Göteborg University, Göteborg, 1996 (unpublished).
[42] E. A. Uehling, Phys. Rev. **48**, 55 (1935).
[43] E. H. Wichmann and N. M. Kroll, Phys. Rev. **101**, 843 (1956).
[44] H. Persson, I. Lindgren, S. Salomonson, and P. Sunnergren, Phys. Rev. A **48**, 2772 (1993).
[45] W. Greiner, B. Müller, and J. Rafelski, *Quantum Electrodynamics of Strong Fields* (Springer-Verlag, Berlin, 1985).
[46] M. Gyulassy, Nucl. Phys. A **244**, 497 (1975).
[47] G. Soff and P. J. Mohr, Phys. Rev. A **38**, 5066 (1988).
[48] A. N. Artemyev, V. M. Shabaev, and V. A. Yerokhin, Phys. Rev. A **56**, 3529 (1997).
[49] H. Persson, S. Salomonson, P. Sunnergren, and I. Lindgren, Phys. Rev. A **56**, R2499 (1997).
[50] J. Aldins *et al.*, Phys. Rev. D **1**, 2378 (1970).
[51] J. Calmet, S. Narison, M. Perrottet, and E. de Rafael, Rev. Mod. Phys. **40**, 21 (1977).
[52] B. E. Lautrup and M. A. Samuel, Phys. Lett. **72B**, 114 (1977).
[53] A. I. Milstein and A. S. Yelkhovsky, Phys. Lett. B **233**, 11 (1989).
[54] A. S. Yelkhovsky and A. I. Milstein, Zh. Eksp. Teor. Fiz. **99**, 1068 (1991) [Sov. Phys. JETP **72**, 592 (1991)].
[55] S. G. Karshenboim (private communication).
[56] V. M. Shabaev (private communication).
[57] P. Raghavan, At. Data Nucl. Data Tables **42**, 189 (1989).
[58] G. Nachtsheim, doctoral thesis, Institut für Angewandte Physik der Universität Bonn, 1980 (unpublished).
[59] L. K. Peker, Nucl. Data Sheets **50**, 137 (1987).
[60] W. R. Johnson and G. Soff, At. Data Nucl. Data Tables **33**, 405 (1985).